

AN UNAMBIGUOUS AND ROBUST FORMULATION FOR WANNIER LOCALIZATION

Kangbo Li,¹ Hsin-Yu Ko,² Robert A. DiStasio Jr.,^{2,*} and Anil Damle^{1,†}

¹*Department of Computer Science, Cornell University, Ithaca, NY 14853, USA*

²*Department of Chemistry and Chemical Biology,
Cornell University, Ithaca, NY 14853, USA*

(Dated: May 18, 2023)

We provide a new variational definition for the spread of an orbital under periodic boundary conditions (PBCs) that is continuous with respect to the gauge, consistent in the thermodynamic limit, well-suited to diffuse orbitals, and systematically adaptable to schemes computing localized Wannier functions. Existing definitions do not satisfy all these desiderata, partly because they depend on an “orbital center”—an ill-defined concept under PBCs. Based on this theoretical development, we showcase a robust and efficient (10x-70x fewer iterations) localization scheme across a range of materials.

Localized Wannier functions (LWFs) offer several theoretical and computational advantages over canonical (Bloch) orbitals in electronic structure calculations of condensed-phase systems. For one, LWFs allow one to probe/characterize the local electronic structure in complex extended systems, thereby enabling chemical bonding analysis (e.g., floating bonds in amorphous Si [1, 2] and Si-C alloys [3]), orbital partitioning (e.g., for computing molecular dipole moments in liquid water [4]), and the construction of chemical-environment-based features and/or targets for machine learning [5]. LWFs also play a critical role in evaluating the bulk properties of materials (e.g., in the modern theory of polarization [6–9] and magnetization [10–14]), predicting and understanding the spectroscopic signatures of condensed matter (e.g., IR [15] and Raman spectra [16]), as well as constructing effective model Hamiltonians (e.g., for quantum transport of electrons [17, 18] and strongly correlated systems [19–22]). Computationally, LWFs also enable large-scale electronic structure calculations to exploit the inherent real-space sparsity (or “near-sightedness” [23]) of exchange-correlation interactions (e.g., in hybrid DFT [24, 25] and GW [26]). As such, a well-defined, robust, and computationally efficient theoretical and algorithmic framework for obtaining LWFs remains highly desirable.

In this Letter, we address two fundamental problems with existing methodologies for obtaining LWFs—one theoretical and one practical. First, we present a new variational definition for the spread of an orbital under PBCs that has several favorable properties, including: continuity with respect to

gauge transforms, consistency in the thermodynamic limit, and applicability to diffuse orbitals. Most importantly, our formulation provides an *unambiguous* ground-truth definition of orbital spread; it sidesteps the fundamentally ill-posed problem of defining an orbital center under PBCs and doing so allows the definition to be unambiguous and gauge continuous. In contrast, prior work based on adaptations of $\langle r^2 \rangle - \langle r \rangle^2$ (e.g., Marzari-Vanderbilt [27]) yield orbital spread ansätze that are not gauge continuous (a property closely related to the complexity of defining a position operator under PBCs as studied by Resta [28, 29]). Given the importance of LWFs, many practically effective “definitions” (or “approximations”) for an orbital spread under PBCs have been proposed [2, 28, 30–33]. While many of these proposals were deemed “equivalent” [34, 35] for generating LWFs, we will show this is not the case.

In practice, our definition of orbital spread could be used directly within a localization scheme. However, it is inherently “global” in k -space and that would make such a scheme marginally more expensive than prior work per iteration. Therefore, we develop a systematic approximation to our spread formulation that is local in k -space and derive its gradient. When paired with techniques from manifold optimization, our approximation results in a favorable localization scheme because: (1) it can be systematically improved if desired, (2) it has an explicit relation to an unambiguous ground truth formula and, therefore, the approximation errors can be quantified, (3) it retains the continuity with respect to gauge transforms of our variational definition, (4) it naturally spans both k -point sampling and Γ -point only calculations, and (5) it exhibits superior performance to prior work. In particular, we show that our method consistently converges in at least an order-of-magnitude

* Corresponding author: distasio@cornell.edu

† Corresponding author: damle@cornell.edu

fewer iterations ($10\times-70\times$) than the widely used Wannier90 code [36] across a diverse set of materials.

Our definition for the spread of an orbital under PBCs is motivated by the variational characterization of the center of an orbital under *open* boundary conditions:

$$\mathbf{c}^* \triangleq \operatorname{argmin}_{\mathbf{r}'} \int \rho(\mathbf{r})(\mathbf{r} - \mathbf{r}')^2 d\mathbf{r} = \int \rho(\mathbf{r})\mathbf{r} d\mathbf{r}, \quad (1)$$

in which $\rho(\mathbf{r})$ is the density of a given Wannier function. Adapting (1) for PBCs leads us to the following *density convolution* (DC), denoted by $\mathcal{S}\rho$:

$$\begin{aligned} (\mathcal{S}\rho)(\mathbf{r}') &\triangleq \int_{\mathbb{S}_{\mathbf{r}'}} \rho(\mathbf{r})(\mathbf{r} - \mathbf{r}')^2 d\mathbf{r} \\ &= \int_{\mathbb{S}_0} \rho(\mathbf{r} + \mathbf{r}')\mathbf{r}^2 d\mathbf{r}, \end{aligned} \quad (2)$$

where \mathbb{S}_0 is the Born-von Karman supercell (i.e., the unit cell replicated with respect to the k -point mesh) and $\mathbb{S}_{\mathbf{r}'}$ is the supercell translated by \mathbf{r}' . The DC center (\mathbf{c}_{DC}) and DC spread (s_{DC}) are then defined as the minimizer and minimum of (2) respectively:

$$\mathbf{c}_{\text{DC}} \triangleq \operatorname{argmin}_{\mathbf{r}'} (\mathcal{S}\rho)(\mathbf{r}') \quad (3)$$

$$s_{\text{DC}} \triangleq \min_{\mathbf{r}'} (\mathcal{S}\rho)(\mathbf{r}'). \quad (4)$$

A key feature of s_{DC} is that it is continuous with respect to the gauge chosen for the Wannier functions. This property arises because s_{DC} is explicitly defined as the minimum of an optimization problem—a continuous quantity with respect to the gauge in this case. This is in stark contrast to commonly used definitions for orbital spread based on $\langle r^2 \rangle - \langle r \rangle^2$ (e.g., [27]) that can be *discontinuous* with respect to the gauge—a property inherited from explicitly depending on the ill-defined notion of an orbital center under PBCs [28, 29]. We sidestep this issue by using a center-independent formulation (cf. (4)); hence, the fact that \mathbf{c}_{DC} is not necessarily continuous with respect to the gauge (as the periodicity implies multiple minimizers) cannot plague s_{DC} even though $s_{\text{DC}} = (\mathcal{S}\rho)(\mathbf{c}_{\text{DC}})$ for any \mathbf{c}_{DC} satisfying (3).

To illustrate this advantage, Fig. 1 illustrates how s_{DC} (and \mathbf{c}_{DC}) vary with respect to the gauge in a simple two-band problem in 1D. For comparison, we also consider the Marzari-Vanderbilt (MV) spread ansatz [27], the optimization of which leads to the so-called maximally localized Wannier functions (MLWFs). Fig. 1(a) and Fig. 1(b) show that s_{MV} is discontinuous (both for $|1\rangle$ and the total spread), which can be directly traced

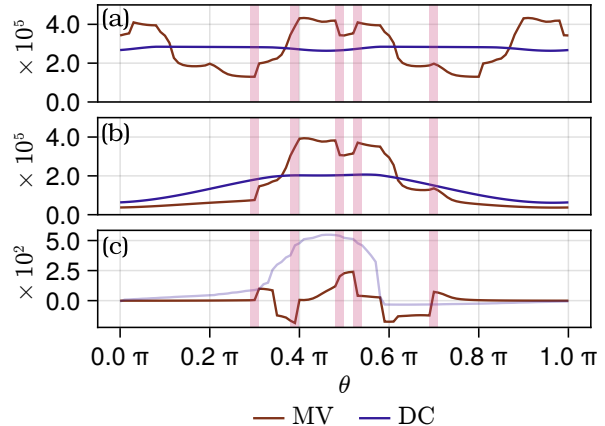


Figure 1. For a simple two-band problem with eight k -points in 1D, we illustrate that s_{DC} varies continuously with respect to the gauge $U(\theta)$ (which is π periodic), while s_{MV} does not. This example contains two Wannier functions $|1\rangle, |2\rangle$ per k -point, and we plot (a) the total spread, (b) the spread of $|1\rangle$, and (c) the center of $|1\rangle$ with discontinuities of s_{MV} (and \mathbf{c}_{MV}) highlighted V.

back to discontinuities in \mathbf{c}_{MV} with respect to the gauge as illustrated in Fig. 1(c). In contrast, s_{DC} is a smooth function of the gauge even though \mathbf{c}_{DC} is ill-behaved.

The DC formulation in (3) and (4) can be intuitively thought of as *implicitly* using the optimal integration boundary (because a periodic convolution is used) when computing an orbital spread in real space. Moreover, numerical evaluation of the DC integral in (2) (e.g., via a Fourier Transform) corresponds to a *spectrally* accurate computation of the orbital spread. This yields a definition that is both consistent in the thermodynamic limit and more accurate for finite-sized domains than common first-order expressions (i.e., as used explicitly by Marzari and Vanderbilt [27] via a finite-difference scheme and implicitly by Resta [28] via the use of a single low-frequency Fourier mode when defining the position operator). Accordingly, s_{DC} is better-suited to quantifying the spread of diffuse orbitals (relative to the unit cell size) and orbitals centered near a unit cell boundary.

To concretely illustrate the validity of s_{DC} for both local and diffuse orbitals, Fig. 2 considers the spread of a square wave (width = $2d$) in a 1D periodic domain. While s_{DC} gives the exact spread ($d^2/3$), s_{MV} is only accurate when d is small relative to the unit cell size and becomes increasingly unreasonable as d grows. This discrepancy can also be seen in real systems containing localized orbitals that are relatively diffuse with respect to the

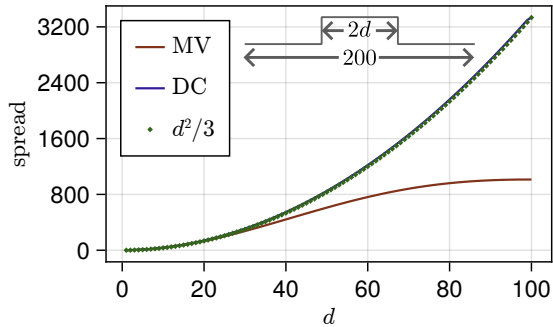


Figure 2. Spread of a square wave in a 1D periodic domain $[-100, 100]$ as a function of the width $2d$. s_{DC} captures the expected $d^2/3$ behavior while s_{MV} only does when d is small relative to the box.

unit cell. A pertinent example is a K-doped molten KCl salt solution ($\text{K}_{33}\text{Cl}_{31}$) [37–39], in which the bipolaron state is close to the conduction band and quite diffuse. Fig. 3 compares s_{MV} and s_{DC} and clearly illustrates that s_{MV} deviates from s_{DC} as the orbitals become more diffuse—in this case, severely underestimating the spread of the bipolaron state by roughly 30%.

One of the most practical and prominent uses for an orbital spread expression is within iterative methods for Wannier localization [34]. While (3) and (4) can easily be computed given an orbital density, they inherently depend on global information (i.e., they are not local operators in k -space), which makes s_{DC} cumbersome to optimize directly. Hence, we now develop a systematic approximation that is center independent, gauge continuous, and consistent in the thermodynamic limit that can be used as a surrogate for s_{DC} within optimization methods; the final spread of a given orbital (and a center, if desired) can then be computed using (4) and (3).

Our derivation I starts with the truncated cosine approximation:

$$r^2 \gtrsim \sum_{\mathbf{b}} 2w_{\mathbf{b}} \text{Re} \left(1 - e^{-i\mathbf{b}^T \mathbf{r}} \right), \quad (5)$$

where \mathbf{b} are selected nearest-neighbor vectors and $w_{\mathbf{b}}$ are the associated weights [27]. This leads to a lower bound for s_{DC} (that is often tight):

$$(S\rho)(\mathbf{r}') \gtrsim \sum_{\mathbf{b}} 2w_{\mathbf{b}} \text{Re} \left(1 - \hat{\rho}(\mathbf{b}) e^{i\mathbf{b}^T \mathbf{r}'} \right), \quad (6)$$

where $\hat{\rho}(\mathbf{b}) = \int_{\mathcal{S}_0} \rho(\mathbf{r}) e^{-i\mathbf{b}^T \mathbf{r}} d\mathbf{r}$ is the unnormalized Fourier transform of $\rho(\mathbf{r})$. For Wannier functions, $\hat{\rho}(\mathbf{b}) = \frac{1}{N} \sum_{\mathbf{k}} M_{n,n}^{\mathbf{k}, \mathbf{k}+\mathbf{b}}$, wherein N is the number of electrons and M is the

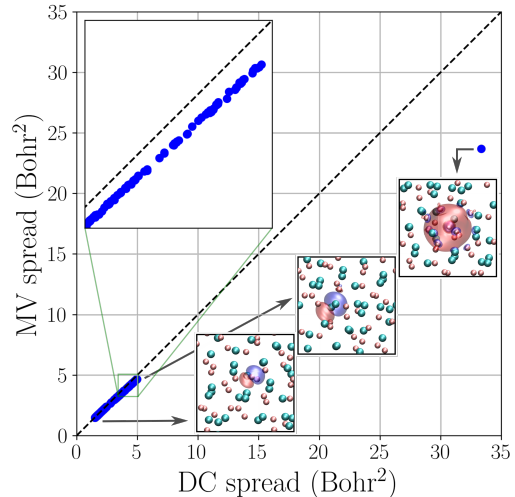


Figure 3. Comparison of s_{DC} and s_{MV} for the localized orbitals in $\text{K}_{33}\text{Cl}_{31}$ computed with `Wannier90` (blue dots). Insets show selected orbital isosurfaces (± 0.0001) overlaid with the unit cell (simple cubic; side length 26.59 Bohr; from Ref. [40]). We observe that s_{MV} deviates from s_{DC} significantly as the orbitals become more diffuse, particularly for the bipolaron state.

set of k -space overlap matrices [27]. We can minimize the right hand side of (6) by choosing \mathbf{r}' to eliminate the phase of $\hat{\rho}(\mathbf{b})$ yielding:

$$s_{DC} \gtrsim s_{TDC} \triangleq \sum_{\mathbf{b}} 2w_{\mathbf{b}} (1 - |\hat{\rho}(\mathbf{b})|), \quad (7)$$

in which s_{TDC} is the *truncated* DC (TDC) approximation (and a formal lower bound) to s_{DC} . In contrast, s_{MV} can either overestimate or underestimate s_{DC} (see Fig. 1). Importantly, s_{TDC} retains the center independence of s_{DC} ; combined with the fact that $\hat{\rho}(\mathbf{b})$ is continuous with respect to the gauge, this implies that s_{TDC} , like s_{DC} , is gauge continuous (Fig. 6).

Interestingly, (7) has appeared as a generalization of Ref. [41] for finite and Γ -point systems by Berghold *et al.* [30], and in the context of disentanglement by Thygesen *et al.* [31] and polarization by Stengel and Spaldin [33]. Without the connection to the underlying DC formulation presented herein, these seminal works did not fully appreciate the advantages of such an approximation as a *center-independent* and *gauge-continuous* definition of orbital spread, particularly in the iterative localization/optimization context (*vide infra*). In fact, this formula was often regarded as being equivalent (or essentially equivalent) to s_{MV} [34].

To highlight the sizable improvement provided by s_{TDC} for iterative localization, we

now compute localized orbitals for a suite of materials using an in-house version of our code [42] and the commonly used Wannier90 code (version 3.1.0) [36]. At its core, our code implements the same gradient-based optimization algorithm as Wannier90, but uses s_{TDC} (instead of s_{MV}) to define the objective function. The TDC scheme introduced herein has a number of favorable properties that allow our code to employ a comparatively simple implementation of manifold optimization in conjunction with standard criteria to reliably determine convergence to localized orbitals.

To compare the convergence behavior of these two objective functions, we performed a challenging benchmark trial based on four diverse materials: Si, Li_2Te , BaTiO_3 , and Cr_2O_3 (Table I). For each material, we performed iterative localization starting from 50 different randomly generated gauges [43]. Fig. 4 provides an empirical characterization of the convergence by plotting the fraction of computations P_c that succeeded within a given number of iterations (with success defined retrospectively as reaching within 0.1% of the minimal objective value observed over all 50 runs). In doing so, we observed that using s_{TDC} consistently reduced the number of iterations required for success by an order of magnitude relative to s_{MV} (i.e., typically $10\times-70\times$ fewer iterations for a fixed P_c) [44]. Our s_{TDC} -based code is robust and converged in all 200 cases. Moreover, it did not achieve success only twice (once for BaTiO_3 and once for Cr_2O_3), indicating that sub-optimal local minima are—in contrary to common belief—likely rare for these materials. While Wannier90 is often (i.e., by default) run for a fixed number of iterations (100 by default), all Wannier90 computations performed in this work were allowed to run for a total of 5,000 iterations; P_c was then evaluated by retrospectively determining the first iteration when success was achieved for each run. Even with this favorable criteria, computations with Wannier90 often failed—e.g., for Cr_2O_3 , Wannier90 never reached success within 1,000 iterations and $P_c \approx 0.75$ even after 5,000 iterations.

To better understand the convergence behavior when using objective functions based on s_{TDC} and s_{MV} , Fig. 5 considers a pair of successful localization computations for Si. Fig. 5(a) shows that s_{MV} for one Si orbital was not monotonic (e.g., between iterations 250 and 300) during the optimization trajectory from Wannier90. Such behavior implies that Wannier90 encountered (and “escaped” from) potentially sub-optimal local minima, consistent with the observations of

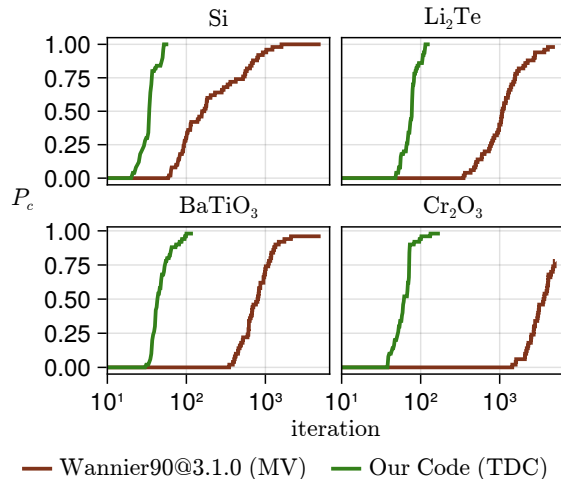


Figure 4. The fraction of orbital localization computations P_c that reached success within a given number of iterations for four diverse materials (with success defined retrospectively as reaching within 0.1% of the minimal objective value observed over 50 runs per material). For fixed P_c values, computations using an s_{TDC} -based objective function consistently succeeded in $10\times-70\times$ fewer iterations than those based on s_{MV} .

Cancès *et al.* [45]; further investigation suggests that these might be non-differentiable (i.e., non-smooth) points where the “gradient” (as defined by the standard MV formulation) is non-vanishing—a challenging scenario for any optimizer. In contrast, Fig. 5(b) shows that s_{TDC} for the analogous orbital monotonically decreases when optimized using our code, which reaches the same localized orbitals (per a visual metric, see inset) as Wannier90 in an order-of-magnitude fewer iterations. Matching our theoretical expectations, s_{TDC} is a lower bound for s_{DC} (which is easily computed for any fixed gauge), with these metrics converging as the orbital becomes more localized. However, s_{MV} severely overestimates the spread of the highlighted localized orbital computed using our code. This discrepancy is due to the distant location of the (necessarily) computed orbital center as seen in Fig. 5(c)—highlighting a potential danger of a center-based definition such as s_{MV} . Consistent with both s_{TDC} and s_{DC} , Fig. 5(d) confirms that our code did indeed compute a local orbital exhibiting exponential decay. As illustrated by Fig. 5(b)-(d) the s_{MV} metric can sometimes fail to recognize localized orbitals, s_{TDC} is not prone to such issues by construction.

We have presented the DC formulation for the spread (and center) of an orbital under PBCs and illustrated its clear theoretical ad-

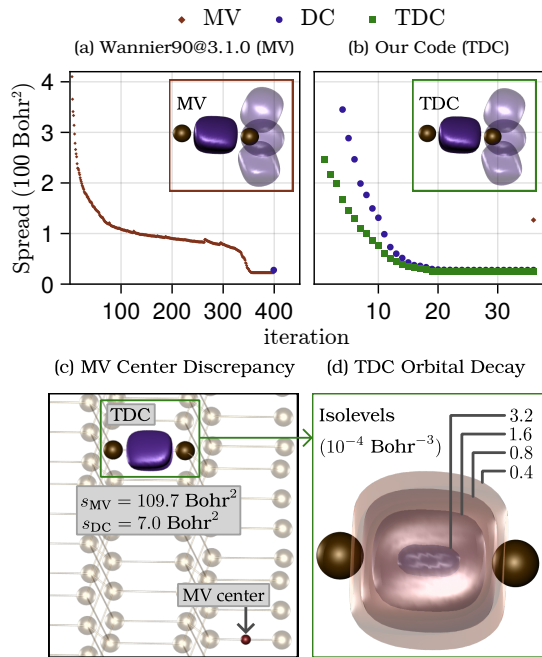


Figure 5. Detailed investigation of two successful localization computations for Si. (a) Non-monotonic decay of s_{MV} for an orbital computed by Wannier90 (dark purple orbital in inset). (b) Evolution of s_{TDC} for the analogous orbital computed by our code, which achieves success in an order-of-magnitude fewer iterations than Wannier90; upon convergence, s_{MV} severely overestimates the spread of this orbital. (c) The distant location of c_{MV} for the orbital in (b) leads to the large discrepancy between the center-based s_{MV} and s_{TDC} (or s_{DC}). (d) Orbital isosurfaces depict the expected (approximate) exponential decay of the orbital in (b) and (c).

vantages (e.g., gauge continuity) relative to prior work. Moreover, preliminary evidence strongly suggests that s_{TDC} (a systematic approximation to s_{DC}) is favorable for use in iterative localization methods—exhibiting significantly improved performance and robustness in challenging scenarios relative to prior work. While we have only discussed insulating systems in this work, entangled systems can also be treated by adapting Ref. [46] to use s_{TDC} and is therefore a potentially interesting direction for future research. Accompanying this work are two Julia packages, `WTP.jl` and `SCDM.jl` [42], that allow researchers to experiment with and expand upon the ideas presented herein.

ACKNOWLEDGMENTS

All authors acknowledge Antoine Levitt for helpful scientific discussions and feedback on an early version of this manuscript. This material is based upon work supported by the National Science Foundation under Grant No. CHE-1945676. RAD also gratefully acknowledges financial support from an Alfred P. Sloan Research Fellowship.

-
- [1] M. Fornari, N. Marzari, M. Peressi, and A. Baldereschi, Wannier functions characterization of floating bonds in a-si, *Computational materials science* **20**, 337 (2001).
 - [2] P. L. Silvestrelli, N. Marzari, D. Vanderbilt, and M. Parrinello, Maximally-localized Wannier functions for disordered systems: Application to amorphous silicon, *Solid State Communications* **107**, 7 (1998).
 - [3] P. Fitzhenry, M. Bilek, N. Marks, N. Cooper, and D. McKenzie, Wannier function analysis of silicon-carbon alloys, *Journal of Physics: Condensed Matter* **15**, 165 (2002).
 - [4] P. Silvestrelli and M. Parrinello, Water dipole moment in the gas and liquid phase, *Phys. Rev. Lett* **82**, 3308 (1999).
 - [5] L. Zhang, M. Chen, X. Wu, H. Wang, E. Weinan, and R. Car, Deep neural network for the dielectric response of insulators, *Physical Review B* **102**, 041121 (2020).
 - [6] R. Resta, Theory of the electric polarization in crystals, *Ferroelectrics* **136**, 51 (1992).
 - [7] R. Resta, Macroscopic polarization in crystalline dielectrics: The geometric phase approach, *Reviews of Modern Physics* **66**, 899 (1994).
 - [8] R. D. King-Smith and D. Vanderbilt, Theory of polarization of crystalline solids, *Physical Review B* **47**, 1651 (1993).
 - [9] D. Vanderbilt and R. D. King-Smith, Electric polarization as a bulk quantity and its relation to surface charge, *Physical Review B* **48**, 4442 (1993).
 - [10] T. Thonhauser, D. Ceresoli, D. Vanderbilt, and R. Resta, Orbital magnetization in periodic insulators, *Physical Review Letters* **95**, 10.1103/physrevlett.95.137205 (2005).
 - [11] D. Xiao, J. Shi, and Q. Niu, Berry phase correction to electron density of states in solids, *Physical Review Letters* **95**, 10.1103/physrevlett.95.137204 (2005).
 - [12] D. Ceresoli, T. Thonhauser, D. Vanderbilt, and R. Resta, Orbital magnetization in crystalline solids: Multi-band insulators, *Chern*

- insulators, and metals, *Physical Review B* **74**, 10.1103/physrevb.74.024408 (2006).
- [13] J. Shi, G. Vignale, D. Xiao, and Q. Niu, Quantum theory of orbital magnetization and its generalization to interacting systems, *Physical Review Letters* **99**, 10.1103/physrevlett.99.197202 (2007).
- [14] I. Souza and D. Vanderbilt, Dichroic f-sum rule and the orbital magnetization of crystals, *Physical Review B* **77**, 10.1103/physrevb.77.054438 (2008).
- [15] M. Sharma, R. Resta, and R. Car, Intermolecular dynamical charge fluctuations in water: A signature of the H-bond network, *Physical Review Letters* **95**, 10.1103/physrevlett.95.187401 (2005).
- [16] Q. Wan, L. Spanu, G. A. Galli, and F. Gygi, Raman spectra of liquid water from *ab initio* molecular dynamics: Vibrational signatures of charge fluctuations in the hydrogen bond network, *Journal of Chemical Theory and Computation* **9**, 4124 (2013).
- [17] A. Calzolari, N. Marzari, I. Souza, and M. Buongiorno Nardelli, *Ab initio* transport properties of nanostructures from maximally localized Wannier functions, *Physical Review B* **69**, 10.1103/physrevb.69.035108 (2004).
- [18] Y.-S. Lee, M. B. Nardelli, and N. Marzari, Band structure and quantum conductance of nanostructures from maximally localized Wannier functions: The case of functionalized carbon nanotubes, *Physical Review Letters* **95**, 10.1103/physrevlett.95.076804 (2005).
- [19] S. Fabris, S. de Gironcoli, S. Baroni, G. Vicario, and G. Balducci, Taming multiple valency with density functionals: A case study of defective ceria, *Physical Review B* **71**, 10.1103/physrevb.71.041102 (2005).
- [20] V. I. Anisimov, A. V. Kozhevnikov, M. A. Korotin, A. V. Lukoyanov, and D. A. Khafizullin, Orbital density functional as a means to restore the discontinuities in the total-energy derivative and the exchange–correlation potential, *Journal of Physics: Condensed Matter* **19**, 106206 (2007).
- [21] T. Miyake and F. Aryasetiawan, Screened Coulomb interaction in the maximally localized Wannier basis, *Physical Review B* **77**, 10.1103/physrevb.77.085122 (2008).
- [22] P. Umari, G. Stenuit, and S. Baroni, Optimal representation of the polarization propagator for large-scale *g* calculations, *Physical Review B* **79**, 10.1103/physrevb.79.201104 (2009).
- [23] E. Prodan and W. Kohn, Nearsightedness of electronic matter, *Proc. Natl. Acad. Sci. U.S.A.* **102**, 11635 (2005).
- [24] H.-Y. Ko, J. Jia, B. Santra, X. Wu, R. Car, and R. A. DiStasio Jr., Enabling large-scale condensed-phase hybrid density functional theory based *ab initio* molecular dynamics. 1. Theory, algorithm, and performance, *Journal of Chemical Theory and Computation* **16**, 3757 (2020).
- [25] H.-Y. Ko, B. Santra, and R. A. DiStasio, Enabling large-scale condensed-phase hybrid density functional theory-based *ab initio* molecular dynamics. 2. Extensions to the isobaric–isoenthalpic and isobaric–isothermal ensembles, *Journal of Chemical Theory and Computation* **17**, 7789 (2021).
- [26] C. Buth, U. Birkenheuer, M. Albrecht, and P. Fulde, *Ab initio* Green’s function formalism for band structures, *Physical Review B* **72**, 10.1103/physrevb.72.195107 (2005).
- [27] N. Marzari and D. Vanderbilt, Maximally localized generalized Wannier functions for composite energy bands, *Physical Review B* **56**, 12847 (1997).
- [28] R. Resta, Quantum-mechanical position operator in extended systems, *Physical Review Letters* **80**, 1800 (1998).
- [29] R. Resta, Electrical polarization and orbital magnetization: The modern theories, *Journal of Physics: Condensed Matter* **22**, 123201 (2010).
- [30] G. Berghold, C. J. Mundy, A. H. Romero, J. Hutter, and M. Parrinello, General and efficient algorithms for obtaining maximally localized Wannier functions, *Physical Review B* **61**, 10040 (2000).
- [31] K. S. Thygesen, L. B. Hansen, and K. W. Jacobsen, Partly occupied Wannier functions: Construction and applications, *Physical Review B* **72**, 10.1103/physrevb.72.125119 (2005).
- [32] P. L. Silvestrelli, Maximally localized Wannier functions for simulations with supercells of general symmetry, *Physical Review B* **59**, 9703 (1999).
- [33] M. Stengel and N. A. Spaldin, Accurate polarization within a unified Wannier function formalism, *Physical Review B* **73**, 10.1103/physrevb.73.075121 (2006).
- [34] N. Marzari, A. A. Mostofi, J. R. Yates, I. Souza, and D. Vanderbilt, Maximally localized Wannier functions: Theory and applications, *Reviews of Modern Physics* **84**, 1419 (2012).
- [35] P. F. Fontana, A. H. Larsen, T. Olsen, and K. S. Thygesen, Spread-balanced Wannier functions: Robust and automatable orbital localization, *Physical Review B* **104**, 10.1103/physrevb.104.125140 (2021).
- [36] G. Pizzi, V. Vitale, R. Arita, S. Blügel, F. Freimuth, G. Géranton, M. Gibertini, D. Gresch, C. Johnson, T. Koretsune, J. Ibañez Azpiroz, H. Lee, J.-M. Lihm, D. Marchand, A. Marrazzo, Y. Mokrousov, J. I. Mustafa, Y. Nohara, Y. Nomura, L. Paulatto, S. Poncé, T. Ponweiser, J. Qiao, F. Thöle, S. S. Tsirkin, M. Wierzbowska, N. Marzari, D. Vanderbilt, I. Souza, A. A. Mostofi, and J. R. Yates, *Wannier90* as a community code: New features and applications, *Journal of Physics: Condensed Matter* **32**, 165902 (2020).
- [37] A. Selloni, P. Carnevali, R. Car, and M. Parrinello, Localization, hopping, and diffusion of electrons in molten salts, *Physical Review*

- Letters **59**, 823 (1987).
- [38] A. Selloni, R. Car, M. Parrinello, and P. Carnevali, Electron pairing in dilute liquid metal-metal halide solutions, *The Journal of Physical Chemistry* **91**, 4947 (1987).
- [39] E. S. Fois, A. Selloni, M. Parrinello, and R. Car, Bipolarons in metal-metal halide solutions, *The Journal of Physical Chemistry* **92**, 3268 (1988).
- [40] P. Pegolo, F. Grasselli, and S. Baroni, Oxidation states, Thouless' pumps, and nontrivial ionic transport in nonstoichiometric electrolytes, *Physical Review X* **10**, 10.1103/physrevx.10.041031 (2020).
- [41] R. Resta and S. Sorella, Electron localization in the insulating state, *Physical Review Letters* **82**, 370 (1999).
- [42] Code available at: <https://github.com/kangboli/WTP.jl> and <https://github.com/kangboli/SCDM.jl>.
- [43] When using randomly projected s -orbitals in Wannier90, the convergence behavior for s_{MV} in Fig. 4 remains effectively unchanged.
- [44] Using s_{DC} as an impartial adjudicator, we verified that the “optimal” local minima found by these two methods have nearly identical spreads (i.e., to within a couple tenths of a percent)—indicating that success for both codes corresponded to computing orbitals with similar locality.
- [45] E. Cancès, A. Levitt, G. Panati, and G. Stoltz, Robust determination of maximally localized Wannier functions, *Physical Review B* **95**, 10.1103/physrevb.95.075114 (2017).
- [46] A. Damle, A. Levitt, and L. Lin, Variational formulation for Wannier functions with entangled band structure, *Multiscale Modeling & Simulation* **17**, 167 (2019).
- [47] The Brillouin zone lattice points are integer combinations of Brillouin zone basis vectors $\mathbf{b} = \sum_i^n n_i \mathbf{b}_i$. The basis vectors are integer (number of k-points along each direction) fractions of the reciprocal lattice basis vectors.
- [48] A. A. Mostofi, J. R. Yates, Y.-S. Lee, I. Souza, D. Vanderbilt, and N. Marzari, Wannier90: A tool for obtaining maximally-localised Wannier functions, *Computer Physics Communications* **178**, 685 (2008).
- [49] P. Absil, *Optimization Algorithms on Matrix Manifolds* (Princeton University Press, 2007).
- [50] J. Hu, X. Liu, Z.-W. Wen, and Y.-X. Yuan, A brief introduction to manifold optimization, *Journal of the Operations Research Society of China* **8**, 199 (2020).
- [51] R. Bergmann, Manopt.jl: Optimization on manifolds in Julia, *Journal of Open Source Software* **7**, 3866 (2022).
- [52] T. Abrudan, J. Eriksson, and V. Koivunen, Conjugate gradient algorithm for optimization under unitary matrix constraint, *Signal Processing* **89**, 1704 (2009).
- [53] J. Manton, Optimization algorithms exploiting unitary constraints, *IEEE Transactions on Signal Processing* **50**, 635 (2002).
- [54] A. Edelman, T. A. Arias, and S. T. Smith, The geometry of algorithms with orthogonality constraints, *SIAM Journal on Matrix Analysis and Applications* **20**, 303 (1998).

Appendix I: Derivation of the TDC spread

We provide a more detailed derivation of the TDC spread and prove that it is a lower bound to the DC spread. First, we make a truncated cosine approximation

$$\mathbf{r}^2 = \sum_{\mathbf{b}} w_{\mathbf{b}} (\mathbf{b}^T \mathbf{r})^2 \gtrsim \sum_{\mathbf{b}} 2w_{\mathbf{b}} \operatorname{Re}(1 - e^{-i\mathbf{b}^T \mathbf{r}}), \quad (\text{I1})$$

where \mathbf{b} are discrete k -points [47] chosen in the neighborhood of the Gamma point (details in [48]), and they satisfy the identity: $\sum_{\mathbf{b}} w_{\mathbf{b}} \mathbf{b} \mathbf{b}^T = I$ [27]. Notably, the approximation (I1) underestimates \mathbf{r}^2 , so applying it to $\mathcal{S}\rho$ (the DC) gives us an underestimate, which we denote as $\mathcal{T}\rho$ (the TDC)

$$(\mathcal{S}\rho)(\mathbf{r}') \gtrsim \sum_{\mathbf{b}} 2w_{\mathbf{b}} \operatorname{Re}(1 - \hat{\rho}(\mathbf{b}) e^{i\mathbf{b}^T \mathbf{r}'}) \triangleq (\mathcal{T}\rho)(\mathbf{r}'), \quad (\text{I2})$$

$$\text{where } \hat{\rho}(\mathbf{b}) = \int_{\mathbb{S}_{\mathbf{r}'}} \rho(\mathbf{r}) e^{-i\mathbf{b}^T \mathbf{r}} d\mathbf{r} = \int_{\mathbb{S}_0} \rho(\mathbf{r}) e^{-i\mathbf{b}^T \mathbf{r}} d\mathbf{r}. \quad (\text{I3})$$

Conveniently, $\hat{\rho}$ is just the unnormalized Fourier transform of ρ , in which the shift of the integration boundary is justified because the integrand is periodic when \mathbf{b} are discrete k -points.

The TDC in Eq. (I2) does not have an apparent analytical minimum, but each term in the sum does have one, and they give us a lower bound on the minimum of the TDC.

$$\min_{\mathbf{r}'} (\mathcal{T}\rho)(\mathbf{r}') \gtrsim \sum_{\mathbf{b}} \min_{\mathbf{r}'} \left(2w_{\mathbf{b}} \operatorname{Re}(1 - \hat{\rho}(\mathbf{b}) e^{i\mathbf{b}^T \mathbf{r}'}) \right) = \sum_{\mathbf{b}} 2w_{\mathbf{b}} (1 - |\hat{\rho}(\mathbf{b})|). \quad (\text{I4})$$

The lower bound is attained if each term in the sum is independently minimized, which corresponds to $\mathbf{b}^T \mathbf{r}' = -\operatorname{Im} \ln \hat{\rho}(\mathbf{b})$. This is a linear system that has a solution for simple lattices, but it can be overdetermined for more complex lattices, so the bound is not always attainable. In either case, we can find a least square solution with the identity: $\sum_{\mathbf{b}} w_{\mathbf{b}} \mathbf{b} \mathbf{b}^T = I$, which gives us the TDC center

$$\mathbf{c}_{\text{TDC}} \triangleq - \sum_{\mathbf{b}} w_{\mathbf{b}} \mathbf{b} \operatorname{Im} \ln \hat{\rho}(\mathbf{b}). \quad (\text{I5})$$

Formally, both the TDC center and the TDC spread are accurate only for well-localized orbitals, in which case the logarithm is stable and the least square procedure has a small residual.

Appendix II: Density of the Wannier Functions

In DFT, the eigenstates of a periodic Hamiltonian take the form of the Bloch orbitals

$$\psi_{n,\mathbf{k}}(\mathbf{r}) = u_{n,\mathbf{k}}(\mathbf{r}) e^{i\mathbf{k}^T \mathbf{r}}, \quad (\text{II1})$$

where \mathbf{k} is a k -point in the first Brillouin zone and $u_{n,\mathbf{k}}(\mathbf{r}) = u_{n,\mathbf{k}}(\mathbf{r} + \mathbf{R})$ is a function periodic under lattice translations by \mathbf{R} . In terms of the Bloch orbitals, the density of a Wannier function ρ_n can be written as

$$\rho_n(\mathbf{r}) = \frac{1}{N} \sum_{\mathbf{k}, \mathbf{k}'} e^{i(\mathbf{k}' - \mathbf{k})^T \mathbf{r}} v_{n,\mathbf{k}}^*(\mathbf{r}) v_{n,\mathbf{k}'}(\mathbf{r}), \quad (\text{II2})$$

where N is the number of k -points sampled in the first Brillouin zone, and the periodic part $u_{n,\mathbf{k}}$ has been transformed by a gauge $v_{n,\mathbf{k}}(\mathbf{r}) = \sum_m U_{n,n}^{\mathbf{k}} u_{m,\mathbf{k}}(\mathbf{r})$. The unnormalized Fourier transform of ρ_n is then

$$\hat{\rho}_n(\mathbf{b}) = \frac{1}{N} \sum_{\mathbf{k}, \mathbf{k}'} \int_{\mathbb{S}_0} e^{i(\mathbf{k}' - \mathbf{k} - \mathbf{b})^T \mathbf{r}} v_{n,\mathbf{k}}^*(\mathbf{r}) v_{n,\mathbf{k}'}(\mathbf{r}) d\mathbf{r} = \frac{1}{N} \sum_{\mathbf{k}} \int_{\mathbb{S}_0} v_{n,\mathbf{k}}^*(\mathbf{r}) v_{n,\mathbf{k}+\mathbf{b}}(\mathbf{r}) d\mathbf{r}. \quad (\text{II3})$$

It is possible for the vector $\mathbf{k} + \mathbf{b}$ in (II3) to be out of the first Brillouin zone. In that case, our notation is to be interpreted as

$$v_{n,\mathbf{k}+\mathbf{b}}(\mathbf{r}) \triangleq \exp(i\mathbf{G}^T \mathbf{r}) v_{n,\mathbf{k}+\mathbf{b}+\mathbf{G}}(\mathbf{r}), \quad (\text{II4})$$

where \mathbf{G} is the reciprocal lattice vector s.t. $\mathbf{k} + \mathbf{b} + \mathbf{G}$ folds into the first Brillouin zone.

Now, using MLWF notations, the unnormalized Fourier transform becomes

$$\hat{\rho}_n(\mathbf{b}) = \frac{1}{N} \sum_{\mathbf{k}} M_{n,n}^{\mathbf{k},\mathbf{k}+\mathbf{b}}, \quad (\text{II5})$$

$$\text{where } M_{m,n}^{\mathbf{k},\mathbf{k}+\mathbf{b}} = \langle v_{m,\mathbf{k}} | v_{n,\mathbf{k}+\mathbf{b}} \rangle = \sum_{p,q} U_{p,m}^{\mathbf{k}*} S_{p,q}^{\mathbf{k},\mathbf{k}+\mathbf{b}} U_{q,n}^{\mathbf{k}+\mathbf{b}}, S_{m,n}^{\mathbf{k},\mathbf{k}+\mathbf{b}} = \langle u_{m,\mathbf{k}} | u_{n,\mathbf{k}+\mathbf{b}} \rangle. \quad (\text{II6})$$

This formula is only notationally different from what Thygesen et al. [31] derived.

Appendix III: The Gradient and Manifold Optimization

Conventionally, to minimize the total spread with respect to the gauge, one derives a *constrained gradient* of the total spread by looking at the effect of adding a constrained first order perturbation to $U^{\mathbf{k}}$. One then applies a gradient descent algorithm that is slightly tweaked to work with the constrained gradient [27, 31]. Although this approach is correct, it does not easily fit into a generic differentiation and optimization framework, making it difficult both to understand and to leverage existing tools.

By contrast, we derive the *Euclidean gradient* (i.e. unconstrained) of the total TDC spread

$$\Omega_{\text{TDC}}(U) = \sum_{n,\mathbf{b}} 2w_{\mathbf{b}}(1 - |\hat{\rho}_n(\mathbf{b})|), \quad (\text{III1})$$

and apply the (Stiefel) manifold optimization. Our description will be procedurally equivalent to the conventional one, but our approach can reach a broader audience and enable the use of automatic differentiation and manifold optimization tools.

To derive the (unconstrained) gradient with respect to $U^{\mathbf{k}}$, we first split $U^{\mathbf{k}}$ and $S^{\mathbf{k},\mathbf{k}+\mathbf{b}}$ into their real and imaginary parts: $U^{\mathbf{k}} = X^{\mathbf{k}} + iY^{\mathbf{k}}$ and $S^{\mathbf{k},\mathbf{k}+\mathbf{b}} = P^{\mathbf{k},\mathbf{k}+\mathbf{b}} + iQ^{\mathbf{k},\mathbf{k}+\mathbf{b}}$. $M_{n,n}^{\mathbf{k},\mathbf{k}+\mathbf{b}}$ can then be expressed as

$$M_{n,n}^{\mathbf{k},\mathbf{k}+\mathbf{b}} = \sum_{r,s} (X_{r,n}^{\mathbf{k}} - iY_{r,n}^{\mathbf{k}}) (P_{r,s}^{\mathbf{k},\mathbf{k}+\mathbf{b}} + iQ_{r,s}^{\mathbf{k},\mathbf{k}+\mathbf{b}}) (X_{s,n}^{\mathbf{k}+\mathbf{b}} + iY_{s,n}^{\mathbf{k}+\mathbf{b}}) = C_{n,n}^{\mathbf{k},\mathbf{k}+\mathbf{b}} + iD_{n,n}^{\mathbf{k},\mathbf{k}+\mathbf{b}}, \quad (\text{III2})$$

$$C_{n,n}^{\mathbf{k},\mathbf{k}+\mathbf{b}} = \sum_{r,s} (P_{r,s}^{\mathbf{k},\mathbf{k}+\mathbf{b}} (X_{r,n}^{\mathbf{k}} X_{s,n}^{\mathbf{k}+\mathbf{b}} + Y_{r,n}^{\mathbf{k}} Y_{s,n}^{\mathbf{k}+\mathbf{b}}) - Q_{r,s}^{\mathbf{k},\mathbf{k}+\mathbf{b}} (X_{r,n}^{\mathbf{k}} Y_{s,n}^{\mathbf{k}+\mathbf{b}} - Y_{r,n}^{\mathbf{k}} X_{s,n}^{\mathbf{k}+\mathbf{b}})), \quad (\text{III3})$$

$$D_{n,n}^{\mathbf{k},\mathbf{k}+\mathbf{b}} = \sum_{r,s} (Q_{r,s}^{\mathbf{k},\mathbf{k}+\mathbf{b}} (X_{r,n}^{\mathbf{k}} X_{s,n}^{\mathbf{k}+\mathbf{b}} + Y_{r,n}^{\mathbf{k}} Y_{s,n}^{\mathbf{k}+\mathbf{b}}) + P_{r,s}^{\mathbf{k},\mathbf{k}+\mathbf{b}} (X_{r,n}^{\mathbf{k}} Y_{s,n}^{\mathbf{k}+\mathbf{b}} - Y_{r,n}^{\mathbf{k}} X_{s,n}^{\mathbf{k}+\mathbf{b}})). \quad (\text{III4})$$

The nontrivial part of our objective function and its derivative can be rewritten as

$$\sum_n |\hat{\rho}_n(\mathbf{b})| = \sum_n \frac{1}{N} \sqrt{\left(\sum_{\mathbf{k}} C_{n,n}^{\mathbf{k},\mathbf{k}+\mathbf{b}} \right)^2 + \left(\sum_{\mathbf{k}} D_{n,n}^{\mathbf{k},\mathbf{k}+\mathbf{b}} \right)^2}, \quad (\text{III5})$$

$$\sum_n \frac{\partial |\hat{\rho}_n(\mathbf{b})|}{\partial U_{i,j}^{\mathbf{k}}} = \sum_{n,\mathbf{h}} \frac{\partial |\hat{\rho}_n(\mathbf{b})|}{\partial C_{n,n}^{\mathbf{h},\mathbf{h}+\mathbf{b}}} \left(\frac{\partial C_{n,n}^{\mathbf{h},\mathbf{h}+\mathbf{b}}}{\partial X_{i,j}^{\mathbf{k}}} + i \frac{\partial C_{n,n}^{\mathbf{h},\mathbf{h}+\mathbf{b}}}{\partial Y_{i,j}^{\mathbf{k}}} \right) + \frac{\partial |\hat{\rho}_n(\mathbf{b})|}{\partial D_{n,n}^{\mathbf{h},\mathbf{h}+\mathbf{b}}} \left(\frac{\partial D_{n,n}^{\mathbf{h},\mathbf{h}+\mathbf{b}}}{\partial X_{i,j}^{\mathbf{k}}} + i \frac{\partial D_{n,n}^{\mathbf{h},\mathbf{h}+\mathbf{b}}}{\partial Y_{i,j}^{\mathbf{k}}} \right). \quad (\text{III6})$$

The derivative of C with respect to X and Y are

$$\frac{\partial C_{n,n}^{\mathbf{h},\mathbf{h}+\mathbf{b}}}{\partial X_{i,j}^{\mathbf{k}}} = \sum_{r,s} P_{r,s}^{\mathbf{h},\mathbf{h}+\mathbf{b}} (\delta_{i,j,\mathbf{k}}^{r,n,\mathbf{h}} X_{s,n}^{\mathbf{h}+\mathbf{b}} + X_{r,n}^{\mathbf{h}} \delta_{i,j,\mathbf{k}}^{s,n,\mathbf{h}+\mathbf{b}}) - Q_{r,s}^{\mathbf{h},\mathbf{h}+\mathbf{b}} (\delta_{i,j,\mathbf{k}}^{r,n,\mathbf{h}} Y_{s,n}^{\mathbf{h}+\mathbf{b}} - Y_{r,n}^{\mathbf{h}} \delta_{i,j,\mathbf{k}}^{s,n,\mathbf{h}+\mathbf{b}}), \quad (\text{III7})$$

$$\frac{\partial C_{n,n}^{\mathbf{h},\mathbf{h}+\mathbf{b}}}{\partial Y_{i,j}^{\mathbf{k}}} = \sum_{r,s} P_{r,s}^{\mathbf{h},\mathbf{h}+\mathbf{b}} (\delta_{i,j,\mathbf{k}}^{r,n,\mathbf{h}} Y_{s,n}^{\mathbf{h}+\mathbf{b}} + Y_{r,n}^{\mathbf{h}} \delta_{i,j,\mathbf{k}}^{s,n,\mathbf{h}+\mathbf{b}}) - Q_{r,s}^{\mathbf{h},\mathbf{h}+\mathbf{b}} (X_{r,n}^{\mathbf{h}} \delta_{i,j,\mathbf{k}}^{s,n,\mathbf{h}+\mathbf{b}} - \delta_{i,j,\mathbf{k}}^{r,n,\mathbf{h}} X_{s,n}^{\mathbf{h}+\mathbf{b}}). \quad (\text{III8})$$

Combining them gives

$$\frac{\partial C_{n,n}^{\mathbf{h},\mathbf{h}+\mathbf{b}}}{\partial U_{i,j}^{\mathbf{k}}} = \sum_{r,s} \left(P_{r,s}^{\mathbf{h},\mathbf{h}+\mathbf{b}} (\delta_{i,j,\mathbf{k}}^{r,n,\mathbf{h}} U_{s,n}^{\mathbf{h}+\mathbf{b}} + U_{r,n}^{\mathbf{h}} \delta_{i,j,\mathbf{k}}^{s,n,\mathbf{h}+\mathbf{b}}) - i Q_{r,s}^{\mathbf{h},\mathbf{h}+\mathbf{b}} (U_{r,n}^{\mathbf{h}} \delta_{i,j,\mathbf{k}}^{s,n,\mathbf{h}+\mathbf{b}} - \delta_{i,j,\mathbf{k}}^{r,n,\mathbf{h}} U_{s,n}^{\mathbf{h}+\mathbf{b}}) \right). \quad (\text{III9})$$

Before we continue, we introduce some tensor symmetries that will simplify our result. Because $S_{m,n}^{\mathbf{k},\mathbf{k}+\mathbf{b}} = \langle u_m^{\mathbf{k}} | u_n^{\mathbf{k}+\mathbf{b}} \rangle = S_{n,m}^{\mathbf{k}+\mathbf{b},\mathbf{k}^*}$, we have the symmetry

$$P_{m,n}^{\mathbf{k},\mathbf{k}+\mathbf{b}} = P_{n,m}^{\mathbf{k}+\mathbf{b},\mathbf{k}}, \quad Q_{m,n}^{\mathbf{k},\mathbf{k}+\mathbf{b}} = -Q_{n,m}^{\mathbf{k}+\mathbf{b},\mathbf{k}}. \quad (\text{III10})$$

The same symmetry applies to C and D for similar reasons. Another symmetry comes from $\rho_n(\mathbf{r})$ being real, which leads to $\hat{\rho}_n(-\mathbf{b}) = \hat{\rho}_n^*(\mathbf{b})$. These symmetries allow us to write the derivative through C as

$$\begin{aligned} \sum_{n,\mathbf{h},\mathbf{b}} \omega_{\mathbf{b}} \frac{\partial |\hat{\rho}_n(\mathbf{b})|}{\partial C_{n,n}^{\mathbf{h},\mathbf{h}+\mathbf{b}}} \frac{\partial C_{n,n}^{\mathbf{h},\mathbf{h}+\mathbf{b}}}{\partial U_{i,j}^{\mathbf{k}}} &= \sum_{\mathbf{b}} \omega_{\mathbf{b}} \left(\frac{\partial |\hat{\rho}_j(\mathbf{b})|}{\partial C_{j,j}^{\mathbf{k},\mathbf{k}+\mathbf{b}}} \sum_s P_{i,s}^{\mathbf{k},\mathbf{k}+\mathbf{b}} U_{s,j}^{\mathbf{k}+\mathbf{b}} + \frac{\partial |\hat{\rho}_j(\mathbf{b})|}{\partial C_{j,j}^{\mathbf{k}-\mathbf{b},\mathbf{k}}} \sum_r P_{r,i}^{\mathbf{k}-\mathbf{b},\mathbf{k}} U_{r,j}^{\mathbf{k}-\mathbf{b}} \right. \\ &\quad \left. - i \frac{\partial |\hat{\rho}_j(\mathbf{b})|}{\partial C_{j,j}^{\mathbf{k}-\mathbf{b},\mathbf{k}}} \sum_r Q_{r,i}^{\mathbf{k}-\mathbf{b},\mathbf{k}} U_{r,j}^{\mathbf{k}-\mathbf{b}} + i \frac{\partial |\hat{\rho}_j(\mathbf{b})|}{\partial C_{j,j}^{\mathbf{k},\mathbf{k}+\mathbf{b}}} \sum_s Q_{i,s}^{\mathbf{k},\mathbf{k}+\mathbf{b}} U_{s,j}^{\mathbf{k}+\mathbf{b}} \right) \\ &= 2 \sum_{\mathbf{b}} \omega_{\mathbf{b}} \frac{\partial |\hat{\rho}_j(\mathbf{b})|}{\partial C_{j,j}^{\mathbf{k},\mathbf{k}+\mathbf{b}}} \sum_s \left(P_{i,s}^{\mathbf{k},\mathbf{k}+\mathbf{b}} U_{s,j}^{\mathbf{k}+\mathbf{b}} + i Q_{i,s}^{\mathbf{k},\mathbf{k}+\mathbf{b}} U_{s,j}^{\mathbf{k}+\mathbf{b}} \right) \\ &= 2 \sum_{\mathbf{b}} \omega_{\mathbf{b}} \frac{\partial |\hat{\rho}_j(\mathbf{b})|}{\partial C_{j,j}^{\mathbf{k},\mathbf{k}+\mathbf{b}}} \sum_s S_{i,s}^{\mathbf{k},\mathbf{k}+\mathbf{b}} U_{s,j}^{\mathbf{k}+\mathbf{b}}, \end{aligned} \quad (\text{III11})$$

where we have replaced $-\mathbf{b}$ with \mathbf{b} because the sum is symmetric ($\sum_{\mathbf{b}} = \sum_{-\mathbf{b}}$). Similarly, the derivative through D can be derived as

$$\begin{aligned} \sum_{n,\mathbf{h},\mathbf{b}} \omega_{\mathbf{b}} \frac{\partial |\hat{\rho}_n(\mathbf{b})|}{\partial D_{n,n}^{\mathbf{h},\mathbf{h}+\mathbf{b}}} \frac{\partial D_{n,n}^{\mathbf{h},\mathbf{h}+\mathbf{b}}}{\partial U_{i,j}^{\mathbf{k}}} &= \sum_{\mathbf{b}} \omega_{\mathbf{b}} \left(\frac{\partial |\hat{\rho}_j(\mathbf{b})|}{\partial D_{j,j}^{\mathbf{k},\mathbf{k}+\mathbf{b}}} \sum_s Q_{i,s}^{\mathbf{k},\mathbf{k}+\mathbf{b}} U_{s,j}^{\mathbf{k}+\mathbf{b}} + \frac{\partial |\hat{\rho}_j(\mathbf{b})|}{\partial D_{j,j}^{\mathbf{k}-\mathbf{b},\mathbf{k}}} \sum_r Q_{r,i}^{\mathbf{k}-\mathbf{b},\mathbf{k}} U_{r,j}^{\mathbf{k}-\mathbf{b}} \right. \\ &\quad \left. + i \frac{\partial |\hat{\rho}_j(\mathbf{b})|}{\partial D_{j,j}^{\mathbf{k}-\mathbf{b},\mathbf{k}}} \sum_r P_{r,i}^{\mathbf{k}-\mathbf{b},\mathbf{k}} U_{r,j}^{\mathbf{k}-\mathbf{b}} - i \frac{\partial |\hat{\rho}_j(\mathbf{b})|}{\partial D_{j,j}^{\mathbf{k},\mathbf{k}+\mathbf{b}}} \sum_s P_{i,s}^{\mathbf{k},\mathbf{k}+\mathbf{b}} U_{s,j}^{\mathbf{k}+\mathbf{b}} \right) \\ &= 2 \sum_{\mathbf{b}} \omega_{\mathbf{b}} \frac{\partial |\hat{\rho}_j(\mathbf{b})|}{\partial D_{j,j}^{\mathbf{k},\mathbf{k}+\mathbf{b}}} \sum_s \left(-i P_{i,s}^{\mathbf{k},\mathbf{k}+\mathbf{b}} U_{s,j}^{\mathbf{k}+\mathbf{b}} + Q_{i,s}^{\mathbf{k},\mathbf{k}+\mathbf{b}} U_{s,j}^{\mathbf{k}+\mathbf{b}} \right) \\ &= -2i \sum_{\mathbf{b}} \omega_{\mathbf{b}} \frac{\partial |\hat{\rho}_j(\mathbf{b})|}{\partial D_{j,j}^{\mathbf{k},\mathbf{k}+\mathbf{b}}} \sum_s S_{i,s}^{\mathbf{k},\mathbf{k}+\mathbf{b}} U_{s,j}^{\mathbf{k}+\mathbf{b}}. \end{aligned} \quad (\text{III12})$$

Finally, the full expression becomes

$$G_{i,j}^{\mathbf{k}} = -2 \sum_{n,\mathbf{b}} \omega_{\mathbf{b}} \frac{\partial |\hat{\rho}_n(\mathbf{b})|}{\partial U_{i,j}^{\mathbf{k}}} = -\frac{4}{N} \sum_{\mathbf{b},s} \omega_{\mathbf{b}} \frac{\hat{\rho}_j^*(\mathbf{b})}{|\hat{\rho}_j(\mathbf{b})|} S_{i,s}^{\mathbf{k},\mathbf{k}+\mathbf{b}} U_{s,j}^{\mathbf{k}+\mathbf{b}}. \quad (\text{III13})$$

Given the gradient $G^{\mathbf{k}}$, any constrained optimization scheme should work. We will use the manifold optimization [49–51], which requires, in addition to the unconstrained gradient, the tangent plane projection and a manifold retraction. In particular, the gauge is constrained on the (power) Stiefel manifold \mathcal{M}^N [52–54], where $\mathcal{M} = \{A \in \mathbb{C}^{N_b \times N_b} : A^\dagger A = I\}$, and N_b is the number of bands. The projection onto \mathcal{M}^N is an antisymmetrization $(G^{\mathbf{k}} - G^{\mathbf{k}\dagger})/2$, and the retraction we use is

$$\text{rt}(U^{\mathbf{k}}, \Delta U^{\mathbf{k}}) = U^{\mathbf{k}} \exp(U^{\mathbf{k}\dagger} \Delta U^{\mathbf{k}}), \quad (\text{III14})$$

where ΔU is the projected gradient step $\alpha (G^{\mathbf{k}} - G^{\mathbf{k}\dagger})/2$ with step size α . The choice of the retraction is not unique as long as it agrees with $U + \Delta U$ to linear order. We chose our retraction to procedurally reproduce the same optimization algorithm as Wannier90, and it does agree with $U + \Delta U$ to linear order

$$U^{\mathbf{k}} \exp(U^{\mathbf{k}\dagger} \Delta U^{\mathbf{k}}) \approx U^{\mathbf{k}} (1 + U^{\mathbf{k}\dagger} \Delta U^{\mathbf{k}}) = U^{\mathbf{k}} + \Delta U^{\mathbf{k}}. \quad (\text{III15})$$

Appendix IV: Materials

We provide a list of materials with the number of k-points and bands in Table. I

Material	# k-points	# bands
Si	64	4
BaTiO ₃	64	9
Li ₂ Te	125	6
Cr ₂ O ₃	216	6

Table I. List of materials: Li₂Te has been previously reported to fail for Wannier90 with random start. Cr₂O₃ is chosen because it is suspected to have multiple good local minima.

Appendix V: Two band problem

For completeness, we evaluate the TDC spread and center for the one dimensional two-band problem and remark that the TDC spread is also continuous with respect to the gauge

$$U(\theta) = \begin{pmatrix} \cos(\theta) & \sin(\theta) \\ -\sin(\theta) & \cos(\theta) \end{pmatrix}. \quad (\text{V1})$$

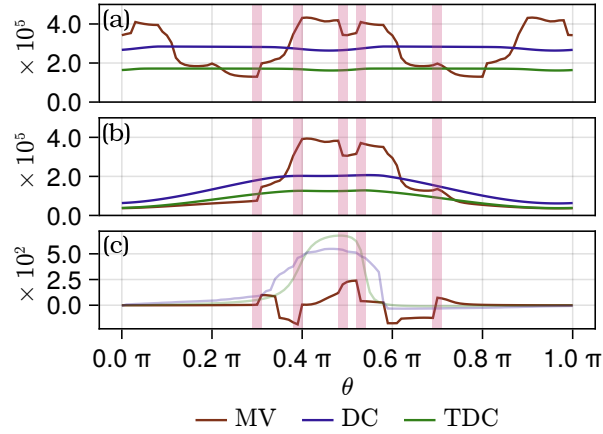


Figure 6. A simple two-band problem with eight k -points in 1D and the TDC spread and center included.